BACKSCATTERING CHARACTERISTICS OF BRIDGES
FROM AIRBORNE FULL-POLARIMETRIC SAR IMAGES

Haruya Hirano[1], Fumio Yamazaki[1] and Wen Liu[1]

[1]Department of Urban Environment Systems, Chiba University
1-33 Yayoi-cho, Inage-ku, Chiba, 263-8522, Japan
Email: hiranoharuya@gmail.com; fumio.yamazaki@faculty.chiba-u.jp; wen.liu@chiba-u.jp

KEY WORDS: Pi-SAR-X2, bridge, full-polarimetry, airborne SAR, backscattering characteristics

ABSTRACT
The inspection of damage situation of bridges is an important issue for the restoration of infrastructures after a disaster strikes. As the first step, this study attempts to grasp backscattering characteristics of bridges over water from a single SAR image. Two full-polarimetric Pi-SAR-X2 airborne SAR images of Tokyo, Japan, were used. The bridge regions of the eight target bridges over the Sumida River were created according to GIS data. A 5-m buffer was applied to expand the region including the layover, double-bounce and triple-bounce components of the bridges. The Pi-SAR-X2 images were decomposed by four scattering components using the G4U method. Then the ratio of each scattering component with respect to the total power, the correlations between HV and VH polarization were calculated within the bridge region. Based on the results, the relationship between the backscattering characteristics, the illumination angle between the bridge-axis and radar's range-direction, and structure types were discussed.

1. INTRODUCTION

Many highway bridges were damaged during the 2011 Tohoku, Japan, earthquake and tsunamis. Due to these damages, traffic networks were suspended and several emergency operations were delayed. Recently, remote sensing technology has been widely used to grasp the damage situations for emergency responses. Synthetic aperture radar (SAR), which can work in all weather conditions and in both daytime and nighttime, is useful to observe the situation of ground surfaces. Airborne platforms have more flexibility than satellites since it can fly over affected areas soon after a disaster strikes. However, it is difficult for airborne platforms to observe the same area in the same acquisition condition twice. Therefore, it is important to extract the damage of bridges only from a post-event airborne SAR image.

Several studies have been conducted which focus on bridge situations using remote sensing images. Shoji et al. (2011) clarified the relationship between the tsunami action and bridge damage mode using optical satellite images. Soergel et al. (2006) decomposed SAR backscatter of bridges into layover, double-bounce and triple-bounce components from airborne interferometric SAR images. Liu et al. (2017) clarified that layover, double-bounce and triple-bounce components of small bridges are overlapped in high-resolution X-band SAR images. Yamazaki et al. (2016) extracted the damaged bridges due to the 2011 Tohoku earthquake using the changes of backscattering coefficients from two temporal high-resolution X-band SAR images.

For the scattering mechanism of SAR images, Cloude et al. (1997) evaluated it using the entropy and alpha degree from the eigenvalues of the coherency matrix. Yamaguchi et al. (2005) decomposed full-polarimetric SAR images into four components using the scattering model matrix, which are easily classify the objects on the ground surface. Chen and Sato (2013) indicated that the double-bounce scattering power of buildings decreases and the surface scattering power increases when urban areas are damaged by tsunamis. However, there is less research working on damage detection of bridges from one post-event SAR image.

After the 2011 Tohoku earthquake and tsunamis, the National Institute of Information and Communications Technology (NICT) carried out an emergency observation of the affected areas using Pi-SAR-X2 sensor. The Pi-SAR-X2 is the second-generation X-band airborne polarimetric and interferometric SAR system developed in 2008 with full polarizations. Unlike single polarization, full-polarimetric SAR images enable us to extract and analyze more detailed information of target objects. Thus, Pi-SAR-X2 images are considered to be suitable for grasping bridge

damages after disasters.

This study attempts to grasp backscattering characteristics of different bridges in Tokyo, Japan, using full-polarimetric Pi-SAR-X2 images. Scattering powers inside expanded bridge footprints are calculated using the decomposed images. The correlation coefficients between HV and VH components within the bridge region are also obtained. After that, the ratios of each component with respect to the total power are calculated as scattering contribution ratios. According to these results, the effects of the structural types and the illumination angle between the bridge-axis and radar's range-direction on the backscattering characteristics of bridges are discussed.

2. STUDY AREA AND IMAGE DATA

In this study, eight bridges over the Sumida River in the Tokyo were adopted as targets. **Figure 1 (a)** shows the study area is located in the central part of Tokyo. Two Pi-SAR-X2 images taken at 5:32 AM on December 22, 2009 and at 3:27 AM on January 10, 2013 were used. These data are Multi-look Ground range Polarimetry (MGP) products including calibrated complex data with full-polarizations (HH/HV/VH/VV). Since the two images observed the same area from the different range direction, the effect of the observe direction on the backscattering characteristics can be confirmed by comparing the two images. **Table 1** shows the detail of the acquisition conditions. After the geocoding step, they were resampled into 0.3 m/pixel in both the range and azimuth directions. **Figure 1 (c-d)** shows the color composite images of the HH, HV and VV polarizations. To keep detailed information of backscatter, a speckle filter was not applied here.

Table 1 Data acquisition conditions

| Date		December 22, 2009	January 10, 2013
Track angle (°)		2.06	-90.1
Incidence angle (°)	Near	41.1	37.8
	Center	42.2	44.3
	Far	43.5	49.8

(a)　　　　　　　　(b)　　　　　　　　(c)　　　　　　　　(d)
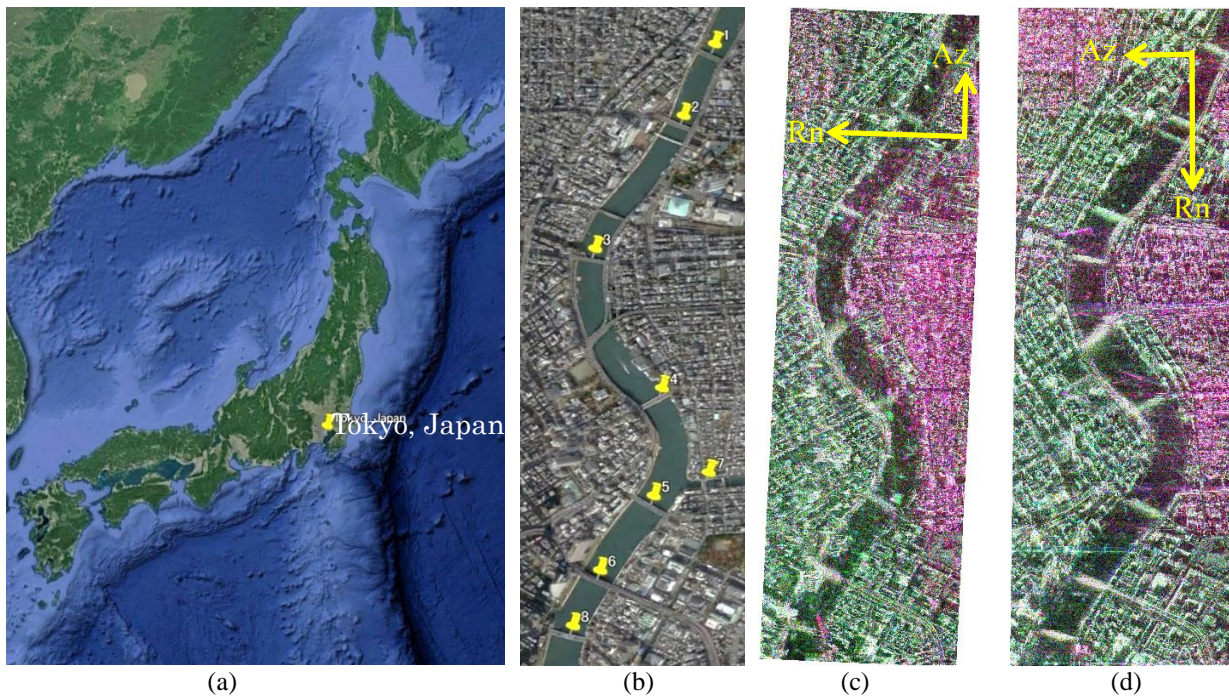
Figure 1 The study area including Sumida-river in Tokyo, Japan, on Google Earth (a) and the eight target bridges (b); color composites of HH (red), HV (green) and VV (blue) polarizations, which were taken on December 22, 2009 (c) and on January 10, 2013 (d).

3. METHODLOGY

First, the bridge outlines were created on ArcGIS according to the road-edge and shoreline data downloaded from the fundamental geospatial data by the Geospatial Information Authority of Japan (GSI, 2017). The region enclosed by the road-edges and shorelines was counted as a bridge over a water surface. Considering to the side-looking natural of the SAR sensor, a 5-m buffer was added as the bridge region. Then a new bridge polygon includes layover, double-bounce and triple-bounce components. Although the Pi-SAR-X2 images have been geocoded according the acquisition condition, the shifts between the SAR images and the map still existed. Thus, several ground control points were selected manually to register the SAR images to the map more precisely. After the registration, the bridge polygons based on the GIS data matched to the SAR images completely. The bridge profiles were calculated within the bridge polygons.

Table 2 shows the observation conditions and the structural types of the target bridges. The illumination angle θ between the bridge-axis and the radar's range-direction was defined as shown **Figure 2**. The correlation between the HV and VH polarizations within the bridge polygon was calculated as a part of the bridge profile and was shown in **Table 2**.
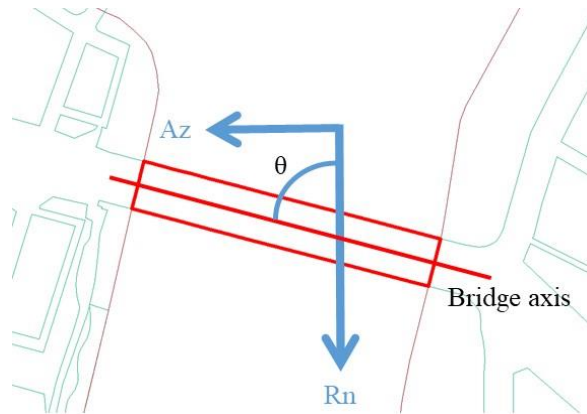
Figure 2 Illumination angle θ between the bridge-axis and the radar's range-direction

Table 2 Illumination angles, correlation coefficients between the HV and VH polarizations, and structural types of the target bridges

Bridge (No.)	December 22, 2009		January 10, 2013		Structural types
	θ (°)	r (HV-VH)	θ (°)	r (HV-VH)	
1	25	0.493	63	0.504	Through arch bridge
2	22	0.429	66	0.495	Upper arch bridge
3	8	0.232	80	0.490	Girder bridge
4	28	0.432	60	0.471	Cable-stayed bridge
5	30	0.473	58	0.480	Suspension bridge
6	26	0.496	62	0.297	Box girder bridge
7	82	0.555	6	0.362	Through arch bridge
8	12	0.456	76	0.454	Through arch bridge

Then the full-polarimetric Pi-SAR-X2 images were decomposed into the 4-component scattering power, which means the double-bounce scattering (Pd), volume scattering (Pv), surface scattering (Ps), Helix scattering (Pc). The decomposition was carried out using the *PolSARpro_v5.1* software developed by the European Space Agency (ESA). The general 4-component scattering power decomposition using the unitary transformation of the coherency matrix (G4U) was adopted as the decomposition method (Singh et al, 2013). The color composites of the decomposed images are shown in **Figure 3**. The ratio of each component with respect to the total power within the bridge polygon was calculated by Eq. (1). Those ratios were also counted as the bridge profiles.

$$\text{Scattering contributi on ratio} = \frac{\text{Pd or Pv or Ps or Pc}}{\text{Total power}} \times 100 \qquad (1)$$
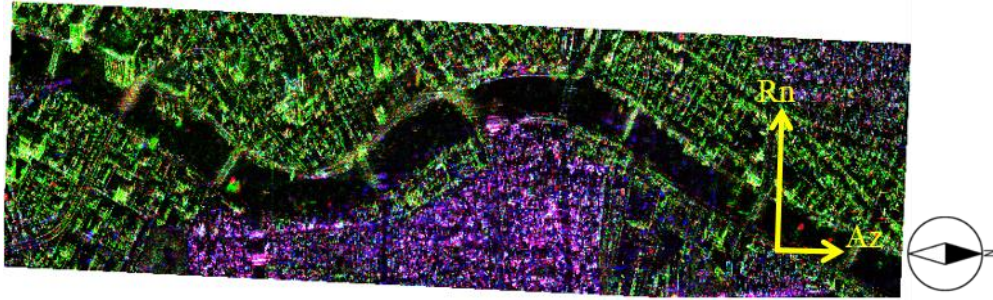
(a) December 22, 2009
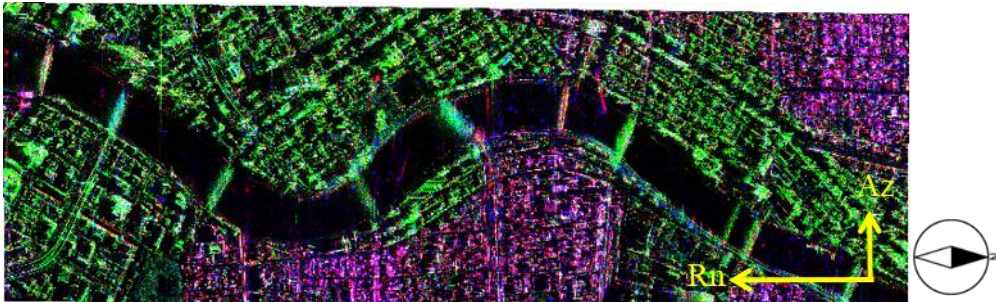
(b) January 10, 2013

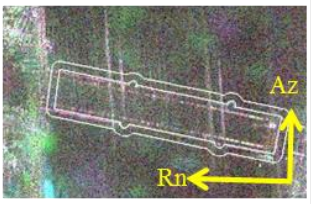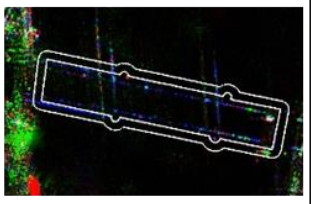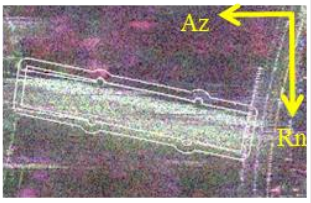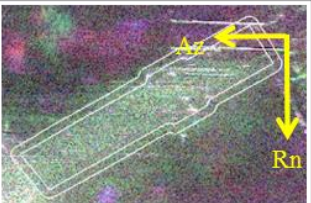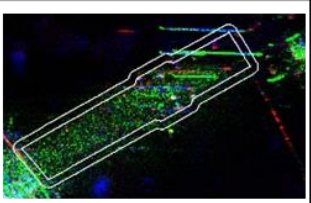**Figure 3** Color composite of the two decomposed airborne SAR images
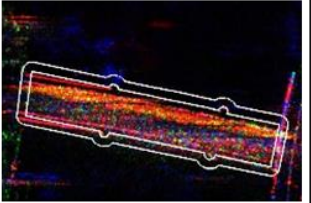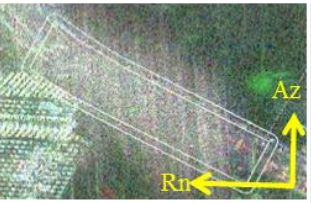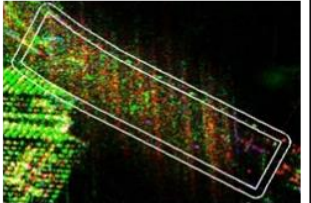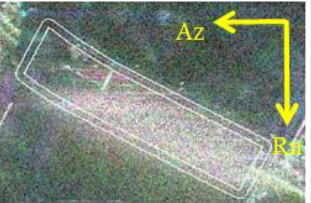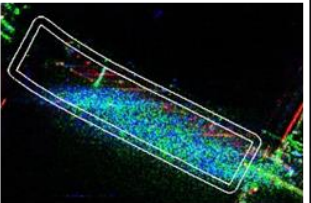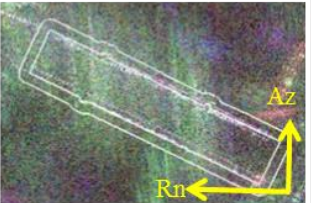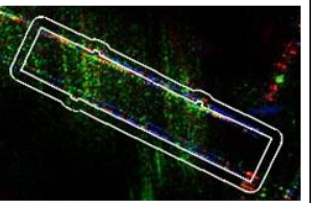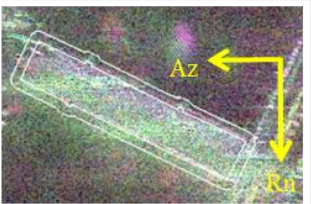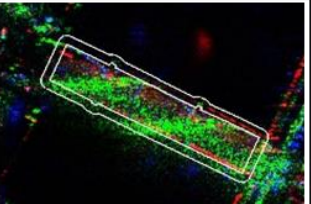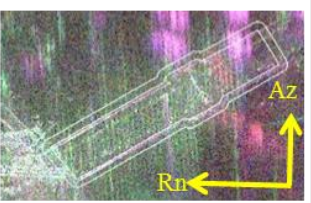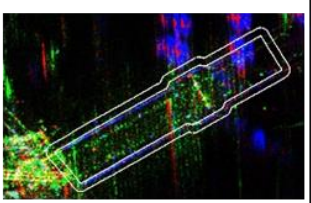
4. RESULT AND DISCUSSION

From **Table 2**, moderately positive correlations between the HV and VH polarizations could be observed. It is known that the HV and VH polarization of the scattering matrix by a monostatic radar should be equal. Although the Pi-SAR-X2 is a monostatic radar, the HV and VH polarizations were different due to the anisotropy of bridges. Therefore, it is needed to discuss the anisotropy of bridges using the eigenvalue analysis in the future.
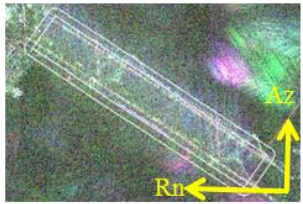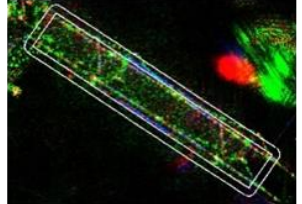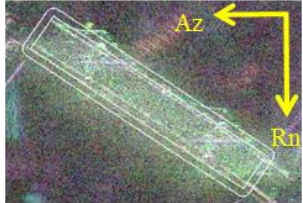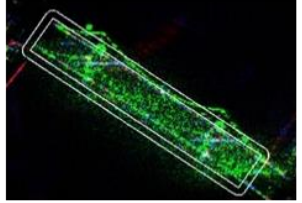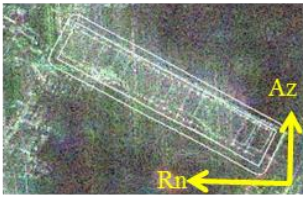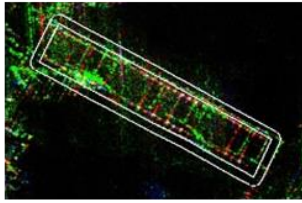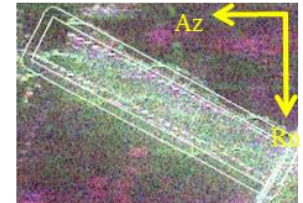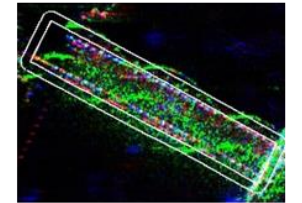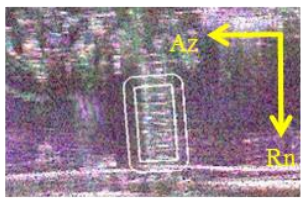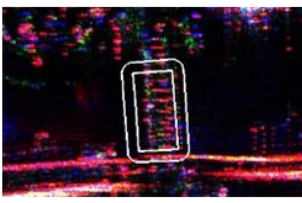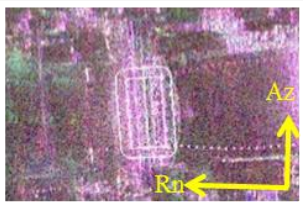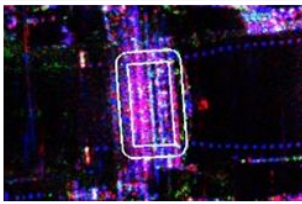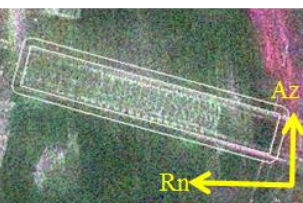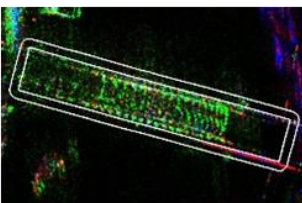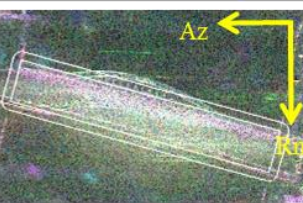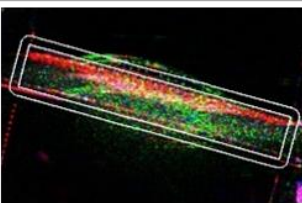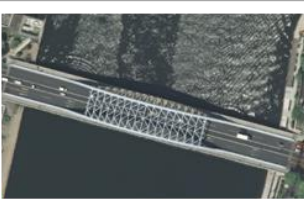
The scattering power for the original polarizations and the decomposed 4-components were discussed hereafter. **Figure 4** and **5** show the comparison of the color composites of the HH, HV, VV polarizations and Pd, Pv, Ps components. The bridges were ordered according to the structural types. The scattering power within each bridge region was averaged and shown in **Table 3**. The contribution ratios obtained by Eq. (1) for each bridge were summarized in **Figure 6**. Since the obtained the Helix scattering power was approximately zero, it was excluded. In addition, the optical images from the Google Earth and the Web Map Service from the GSI are added in **Figure 4** and **5** in order to compare with the SAR images.

The bridge No. 3 is a simple girder bridge composed by only girder and slabs. The ratio of the surface scattering was highest among the three scattering components when the illumination angle was 8°. Strong surface scattering occurred along the side face of the bridge. A low backscatter could be confirmed on the slabs due to specular reflection. On the other hand, the ratio of the double-bounce scattering was highest when the illumination angle was 80°. It could be noted that the double-bounce occurred easier when the illumination angle is close to 90°.

The bridge No. 6 is a box-girder bridge, whose structural type is similar to the girder bridge. However, this bridge has two slabs overlapped up and down. Different from the bridge No.3, the ratio of the double-bounce scattering was high when the illumination angle was 26°, whereas the ratio of the surface scattering was high when the angle was 62°. Since the slab of this bridge is thicker than the girder bridge No. 3, the double-bounce from the side was stronger than that of the bridge No. 3 when the illumination angle was 26°. Strong double-bounce scattering from the electric poles and traffic signs can be confirmed in the both SAR images in **Figure 4**. These superstructures were also

Bridge No.	θ (°)	R:HH G:HV B:VV	R:Pd G:Pv B:Ps	Google Earth or GSI Maps
No. 3 Girder bridge	8			
	80			
No. 6 Box girder bridge	26			
	62			
No. 2 Upper arch bridge	22			
	66			
No. 4 Cable-stayed bridge	28			
	60			

Figure 4 Comparison of the color composite of HH, HV and VV polarizations, that of Pd, Pv, Ps scattering components and optical images from Google Earth or GSI, for the bridges No. 2, No. 3, No. 4 and No. 6.

Bridge No.	θ (°)	R:HH G:HV B:VV	R:Pd G:Pv B:Ps	Google Earth or GSI Maps
No. 5 Suspension bridge	30			
	58			
No. 1 Through arch bridge	25			
	63			
No. 7 Through arch bridge	6			
	82			
No. 8 Through arch bridge	12			
	76			

Figure 5 Comparison of the color composite of HH, HV and VV polarizations, that of Pd, Pv, Ps scattering components and optical images from Google Earth or GSI, for the bridges No. 1, No. 5, No. 7 and No. 8.

Table 3 Scattering powers of each components within the bridge region with the illumination angle θ and structural types

| Bridges No. and structural types	θ (°)	Pd (dBm²)	Pv (dBm²)	Ps (dBm²)	Total power (dBm²)
No. 3 Girder bridge	8	0.121	0.053	0.210	0.384
	80	1.277	0.098	0.193	1.568
No. 6 Box girder bridge	26	0.693	0.363	0.199	1.255
	62	0.204	0.224	0.441	0.869
No.2 Upper arch bridge	22	0.254	0.131	0.182	0.567
	66	0.474	0.267	0.118	0.859
No. 4 Cable-stayed bridge	28	0.375	0.219	0.822	1.416
	60	0.230	0.188	0.176	0.593
No. 5 Suspension bridge	30	0.490	0.248	0.431	1.169
	58	0.217	0.257	0.244	0.718
No. 1 Through arch bridge	25	1.235	0.240	0.194	1.669
	63	0.695	0.371	0.764	1.831
No. 7 Through arch bridge	6	0.884	0.050	0.156	1.090
	82	4.105	0.206	19.665	23.976
No. 8 Through arch bridge	12	0.333	0.259	0.257	0.850
	76	1.114	0.226	0.182	1.522

considered as the reason of the large double-bounce contribution. Since the odd number time reflections occurred from the bottom of the upper slab, which were counted as surface scattering, they contributed to the high ratio when the illumination angle was large.

The bridge No. 2 is an upper arch bridge including arch structure beneath the road. The ratios of the double-bounce scattering were highest in the both cases when the illumination angles were 22° and 66°. Owing to the structure beneath the road, the double-bounce scattering from the side face was larger than that of the girder bridge No. 3. In addition, the volume scattering occurred within the arch also showed high contribution. However, the trend of the contribution ratio changes when the illumination angle increases was similar than that of the girder bridge No. 3.

The bridge No. 4 is a cable-stayed bridge, in which the slab is supported by the slant cables from tower. The surface scattering dominated the reflection when the illumination angle was 28°. When the angle was 60°, the ratio of the three component were almost the same. The trend of the ratio change when the angle increases was also similar to that of the bridge Nos. 3 and 2. However, the volume scattering could be confirmed in the both Pi-SAR-X2 images. This is considered due to the interaction with the cables.

The bridge No. 5 is a suspension bridge, in which the slab is supported by vertical cables from towers. The volume scattering occurred between the cables and towers could be recognized from the both SAR images. Since the vertical cables show the double-bounce scattering more than the oblique cables, the ratio of the double-bounce scattering was larger than that of the bridge No. 4 when the illumination angle was 30°. When the illumination angle was 58°, the ratio of the three component were almost the same, similar to that of the bridge No. 4.

The bridge Nos. 1, 7 and 8 are through arch bridges, where the arch components are over the road. The same trend of the ratio changes when the illumination angle increases was observed from the bridge Nos. 1 and 7. Strong double-bounce scattering occurred from the arch structures when the illumination angle was small. When the angle was close to 90°, the surface scattering became stronger. However, the trend of the ratio change was opposed to that of the bridge No. 8. A similar contribution ratio of each component was observed for the small illumination angle, and strong double-bounce scattering was observed for the large angle. Although the three bridges are the same structural types, arch superstructures are different. The arch structure of the bridge No. 8 is in the middle of the slab with high density pipes. This structure might cause the difference among the bridge No. 8 and Nos. 1, 7. Since the illumination angles of the bridge No. 7 were close to parallel or perpendicular, the volume scatterings were small. But, the volume scattering could be observed for the bridge Nos. 1 and 8 in the both SAR images.

(a)

(b)
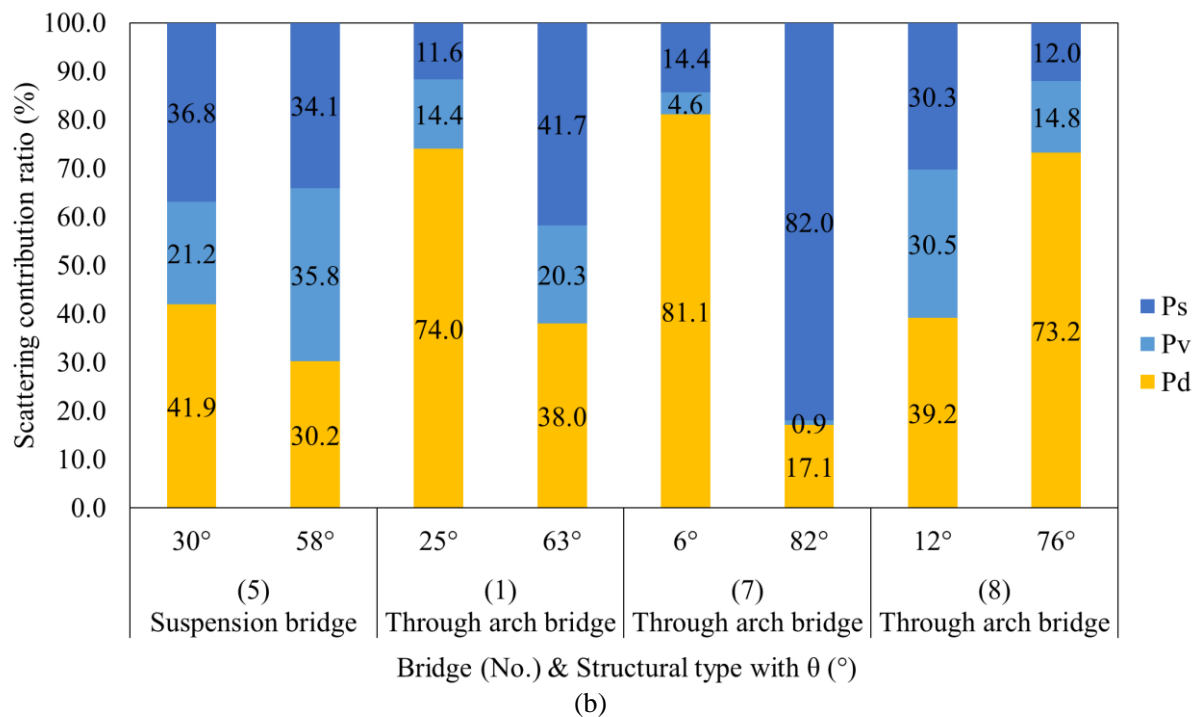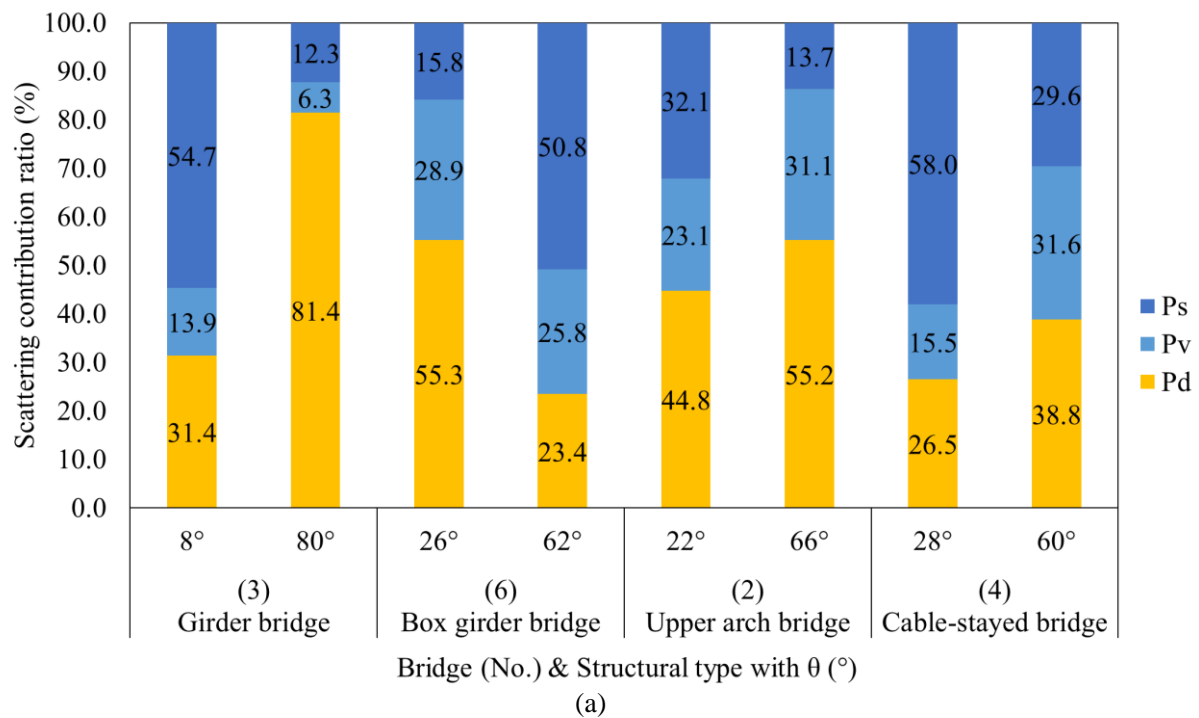
Figure 6 Contribution ratios of each scattering component for the target bridges, which were ordered by the structural types

5. CONCLUSIONS

In this study, the backscattering characteristics of eight bridges over the Sumida River in Tokyo, Japan, were investigated using full-polarimetric airborne X-band SAR images. Two Pi-SAR-X2 images with the different observation angles were decomposed into four components using the G4U method. The bridge regions were created using the GIS data by the GSI with a 5-m buffer. The ratio of each scattering component with respect to the total power was calculated within the bridge region. Then the relationship between the ratio change and the illumination angle, bridge structural types was discussed.

As the result, it is found that relationship between the HV polarization scattering and VH polarization scattering inside of a bridge region has a moderate positive correlation. Also, it is found that the backscattering characteristics of bridges basically follow the scattering mechanism of bridge girders. This is because every bridge has a girder and a slab regardless of its structural type. However, the trend of the ratio changes in case that a bridge has additional components such as arches, truss, towers, cables, handrails, electric poles and traffic signs. When these components exist, the ratio of double-bounce scattering becomes higher as the illumination angle to the components is close to 0°. On the other hand, the ratio of surface scattering becomes higher when the angle is close to 90°. Several components such as arches, towers and cables might cause the volume scattering in the range of the angles, 10° to 80°.

When bridges are damaged by earthquakes and tsunamis, their backscattering characteristics might be changed after the event. Although this study focused on only non-damaged bridges, the backscattering characteristics of damaged bridges will be examined by the same method in the near future. Then the method to extract damaged bridges from a single SAR image will be developed. In addition, the applications of the polarization correlation analysis and eigenvalue analysis will be considered in the future work.

6. ACKNOWLEDGEMENTS

7. REFERENCES

Chen, S., Sato, M., 2013, Tsunami damage investigation of built-up areas using multitemporal spaceborne full polarimetric SAR images, IEEE transactions on Geoscience. Remote Sensing, 51 (4), pp. 1985-1997.

Cloude, S., Pottier, E., 1997, An entropy based classification scheme for land applications of polarimetric SAR, IEEE transactions on Geoscience. Remote Sensing, 35 (1), pp. 68-78.

Geospatial Information Authority of Japan (GSI), 2017, Fundamental Geospatial Data, http://www.gsi.go.jp/kiban/ (accessed on 22 September 2017)

Geospatial Information Authority of Japan (GSI), 2017, GSI Maps, http://www.gsi.go.jp/kiban/ (accessed on 22 September 2017)

Liu, W., Sawa, K., Yamazaki, F., 2017. Backscattering characteristics of bridges from high-resolution X-band SAR imagery, International Symposium on Remote Sensing, D-24, pp. 324-327.

Singh, G., Yamaguchi, Y., Park, S., 2013, General four-component scattering power decomposition with unitary transformation of coherency matrix, IEEE transactions on Geoscience. Remote Sensing, 51 (5), pp. 3014-3022.

Shoji, G., Takahashi, K., Nakamura, T., 2012, Tsunami Damage Assessment on Bridge Structures Subjected to the 2011 off the Pacific Coast of Tohoku Earthquake Tsunami (in Japanese), Journal of Japan Association for Earthquake Engineering, 12 (6), pp. 104-119.

Soergel, U., Gross, H., Thiele, A., Thoennessen, U., 2006. Extraction of bridges over water in multi-aspect high-resolution InSAR data, International Archives of the Photogrammetry, Remote Sensing and Spatial Information Sciences, XXXVI (3), pp. 185-190.

Yamaguchi, Y., Moriyama, T., Ishido, M., Yamada, H., 2005, Four-component scattering model for polarimetric SAR image decomposition, IEEE transactions on Geoscience. Remote Sensing, 43 (8), pp. 1699-1706.

Yamazaki, F., Inoue, K., Liu, W., 2016, Damage assessment of bridges using spatial characteristics of high-resolution satellite SAR intensity images, Meccanica dei Materiali e delle Strutture, VI (1), pp. 163-170.